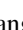

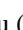





## Nuclear temperature and its dependence on the source neutron-proton asymmetry deduced using the Albergo thermometer

Y. Huang (黄宇),<sup>1</sup> H. Zheng (郑华) <sup>2</sup>, R. Wada,<sup>3,4</sup> X. Liu (刘星泉),<sup>1,\*</sup> W. Lin (林炜平) <sup>1,†</sup>, G. Qu (曲国峰),<sup>1</sup> M. Huang (黄美容),<sup>5</sup> P. Ren (任培培),<sup>1</sup> J. Han (韩纪锋),<sup>1</sup> A. Bonasera,<sup>3,6</sup> K. Hagel,<sup>3</sup> M. R. D. Rodrigues <sup>7</sup>, S. Kowalski <sup>8</sup>, T. Keutgen <sup>9</sup>, M. Barbui,<sup>3</sup> and J. B. Natowitz <sup>3</sup>

<sup>1</sup>Key Laboratory of Radiation Physics and Technology of the Ministry of Education, Institute of Nuclear Science and Technology, Sichuan University, Chengdu 610064, China

<sup>2</sup>School of Physics and Information Technology, Shaanxi Normal University, Xi'an 710119, China

<sup>3</sup>Cyclotron Institute, Texas A&M University, College Station, Texas 77843, USA

<sup>4</sup>School of Physics, Henan Normal University, Xixiang 453007, China

<sup>5</sup>College of Physics and Electronics Information, Inner Mongolia University for Nationalities, Tongliao 028000, China

<sup>6</sup>Laboratori Nazionali del Sud, INFN, via Santa Sofia, 62, 95123 Catania, Italy

<sup>7</sup>Instituto de Física, Universidade de São Paulo, Caixa Postal 66318, CEP 05389-970, São Paulo, São Paulo, Brazil

<sup>8</sup>Institute of Physics, Silesia University, Katowice, Poland

<sup>9</sup>FNRS and IPN, Université Catholique de Louvain, B-1348 Louvain-Neuve, Belgium



(Received 17 September 2020; revised 25 October 2020; accepted 18 December 2020; published 5 January 2021)

Albergo thermometers with double isotope, isotone, and isobar yield ratio pairs with one proton and/or neutron difference are investigated. Without any extra sequential decay correction, a real temperature value of  $4.9 \pm 0.5$  MeV is deduced from the yields of the experimentally reconstructed primary hot intermediate mass fragments (IMFs) from  $^{64}\text{Zn} + ^{112}\text{Sn}$  collisions at 40 MeV/nucleon using the Albergo thermometer for the first time. An experimental sequential decay correction from the apparent temperatures to the real ones for 12 other reaction systems with different neutron-proton ( $N/Z$ ) asymmetries in the same experiment,  $^{70}\text{Zn}$ ,  $^{64}\text{Ni}$  on  $^{112,124}\text{Sn}$ ,  $^{58,64}\text{Ni}$ ,  $^{197}\text{Au}$ , and  $^{232}\text{Th}$  at 40 MeV/nucleon, is performed using an empirical correction factor approach of Tsang *et al.* [*Phys. Rev. Lett.* **78**, 3836 (1997)] with the deduced 4.9-MeV temperature value. The dependence of nuclear temperature on the source  $N/Z$  asymmetry is further investigated using these deduced real source temperature values from the present 13 systems. It is found that the deduced real source temperatures at the present source  $N/Z$  range show a rather weak dependence on the source  $N/Z$  asymmetry. By comparison between our previous results and those from other independent experiments, a consistent description for the  $N/Z$  asymmetry dependence of nuclear temperature is addressed.

DOI: [10.1103/PhysRevC.103.014601](https://doi.org/10.1103/PhysRevC.103.014601)

### I. INTRODUCTION

Nuclear temperature was first introduced to describe the formation and decay of a compound nucleus in the 1930s [1,2], and later extended to nuclear reactions to gain insights into the characteristics of the fragmenting source and the reaction dynamics [3,4]. To extract temperature information experimentally, several nuclear “thermometers” have been proposed based on various experimental observables, i.e., energy spectra [5,6], momentum fluctuations [7], double isotope yield ratios [8], excited state populations [9], etc. Among them, the double isotope yield ratio thermometer, which is often referred as the Albergo thermometer, has a wide application for different reactions at different incident energies. When deducing the temperature using the Albergo thermometer (as well as other thermometers), one of the

significant complications in nuclear reactions is the sequential decay processes. That is, as the fragments produced in the reactions at freeze-out are generally highly excited, they will undergo sequential decays. Thus, the measured isotope yields are often significantly perturbed by the sequential decays, resulting in a serious inaccuracy in the temperature determination. The temperature deduced from the experimentally measured isotope yields is therefore called “apparent temperature,” whereas the temperature before the sequential decays is called “real (source) temperature” (similarly hereinafter). To take into account the sequential decay effect, two general approaches [10,11] have been developed to achieve the sequential decay correction from the apparent temperatures to the real ones. The former is based on the theoretical calculations [10], whereas the latter uses the empirical correction factor deduced from experiments [11]. In our previous work [12], a kinematical focusing technique has been proposed and employed to experimentally reconstruct the yields of primary hot intermediate mass fragments (IMFs, i.e.,  $Z \geq 3$ ) from  $^{64}\text{Zn} + ^{112}\text{Sn}$  collisions at 40 MeV/nucleon. The available

\*liuxingquan@scu.edu.cn

†linwp1204@scu.edu.cn

reconstructed IMF yields may provide another opportunity to deduce the real source temperature using the Albergo thermometer, without extra sequential decay corrections.

During the heavy ion collisions at intermediate energies, IMFs are copiously produced in multifragmentation processes [13–16]. It is generally expected that the overlap region of the composite system of projectile and target nuclei is first compressed and excited in the early stage of the reaction for central or semi-central collisions, and then the hot-dense nuclear system expands and breaks up. At the early rapid expansion stages many light particles are emitted from rather hot regions of the system at high temperatures, whereas the IMF emissions are with a tendency of coming from cold regions of the system at late stages. This scenario finds support from the experimental observation of Tsang and Xi *et al.* [11,17] that temperatures involving heavier isotopes are lower than those with lighter ones. In a series of our works [18–21], we established a method, a so-called self-consistent method, to extract consistently the temperature, density, and symmetry energy at the same time, making the use of the nature that the isotope distribution widths of IMFs are mainly governed by the symmetry energy at given density and temperature during the fragment formation. In these studies, a low-temperature of around 5–6 MeV and a low density of  $\rho/\rho_0 \approx 0.6$  were obtained, indicating that IMF isotope distributions are attained at subsaturation densities, as well as supporting a IMF formation at late stages. This scenario was further confirmed by the theoretical study with the events of  $^{40}\text{Ca} + ^{40}\text{Ca}$  central collisions at 35 to 300 MeV/nucleon using the antisymmetrized molecular dynamics (AMD) [22,23]. The Albergo thermometers use the isotope yields, and therefore those involving IMF yields can probe the temperatures at late stages when the nuclear matter reaches at an expanding freeze-out volume.

Of broader interest, the study on the dependence of nuclear temperature on the source neutron-proton ( $N/Z$ ) asymmetry provides crucial information on the  $N/Z$  asymmetry dependence of the nuclear forces, the nuclear equation of state, and the postulated nuclear liquid-gas phase transition [4,24–27]. However, up to now large uncertainties in the nuclear temperature  $N/Z$  asymmetry dependence still remain. On one hand, sequential decay process significantly influences the performance of nuclear thermometers [5–9,28], and on the other hand, the applications of different thermometers in the experimental temperature determination [7,29,30] and the different modeling assumptions in the calculations [31–34] also result in the conflicting conclusions in both experiment and theory. Recently, we studied the source  $N/Z$  asymmetry dependence of nuclear temperature with measured light charged particles (LCPs) and IMFs from 13 reaction systems with different  $N/Z$  asymmetries,  $^{64}\text{Zn}$  on  $^{112}\text{Sn}$ , and  $^{70}\text{Zn}$ ,  $^{64}\text{Ni}$  on  $^{112,124}\text{Sn}$ ,  $^{58,64}\text{Ni}$ ,  $^{197}\text{Au}$ ,  $^{232}\text{Th}$  at 40 MeV/nucleon [30,35]. In those works, the Albergo thermometer was used to deduce the temperature values. To further isolate the reaction mechanisms involved in the reaction products, the fragmenting sources were characterized using a moving source fit [36]. An “indirect” method used by Sfienti *et al.* in Ref. [37] was adopted to take into account the sequential decay effect. That is, instead of using the Albergo thermometer as an absolute

thermometer, we used it as a relative thermometer. A rather weak  $N/Z$  asymmetry dependence of the source temperature for both LCPs and IMFs was qualitatively inferred at the measured source  $N/Z$  range from the extracted weak  $N/Z$  asymmetry dependence of the apparent temperature and the weak  $N/Z$  asymmetry dependence of the relative temperature change by the sequential decay effects predicted by the models [23,38,39].

In this article, we deduce real temperature from the experimentally reconstructed primary hot IMF yields from the collisions of  $^{64}\text{Zn} + ^{112}\text{Sn}$  at 40 MeV/nucleon using the Albergo thermometer for the first time. Not only double isotope yield ratio pairs but also double isotone and isobar yield ratio pairs are examined and used in this work. We then explore the  $N/Z$  asymmetry dependence of nuclear temperature using the Albergo thermometer as an absolute thermometer. For comparison with our previous results, the same IMF yield data from  $^{64}\text{Zn}$  on  $^{112}\text{Sn}$ , and  $^{70}\text{Zn}$ ,  $^{64}\text{Ni}$  on  $^{112,124}\text{Sn}$ ,  $^{58,64}\text{Ni}$ ,  $^{197}\text{Au}$ ,  $^{232}\text{Th}$  at 40 MeV/nucleon [30,35] are used. For the 12 systems (excluding the  $^{64}\text{Zn} + ^{112}\text{Sn}$  system) in which the experimentally reconstructed primary hot IMFs are not available, the empirical correction factor approach of Tsang *et al.* [11] is applied to achieve the sequential decay correction from the apparent temperatures to the real ones. This strategy, comparing with that adopted in our previous works, is direct, and the  $N/Z$  asymmetry dependence of nuclear temperature can be deduced quantitatively. This article is organized as follows. In Sec. II, the experiment and data analysis are briefly introduced. In Sec. III, the Albergo thermometer is investigated; the  $N/Z$  asymmetry dependence of the real temperature is deduced and discussed. In Sec. IV, a summary is given.

## II. EXPERIMENT AND DATA ANALYSIS

Even though detailed descriptions were given elsewhere [12,30,35], the experimental details and the data analysis are briefly introduced in this section, since they closely relate to the analysis and results presented in the following sections. The experiment was performed at the K-500 superconducting cyclotron facility at Texas A&M University using  $^{64,70}\text{Zn}$  and  $^{64}\text{Ni}$  beams irradiated on  $^{58,64}\text{Ni}$ ,  $^{112,124}\text{Sn}$ ,  $^{197}\text{Au}$ , and  $^{232}\text{Th}$  targets at 40 MeV/nucleon. Only certain selected targets were used for each beam due to the limited beam time. During the experiment, IMFs were detected by a detector telescope placed at  $20^\circ$ . The telescope consisted of four Si detectors. Each Si detector was  $5 \times 5$  cm. The nominal thicknesses were 129, 300, 1000, and  $1000 \mu\text{m}$ , respectively. All four Si detectors were segmented into four sections and each quadrant had a  $5^\circ$  opening in polar angle. The telescope provided the main trigger for all detected events. Typically, six to eight isotopes for atomic numbers  $Z$  up to  $Z = 18$  were clearly identified with the energy threshold of 4–10 MeV/nucleon, using the  $\Delta E - E$  technique for any two consecutive detectors. The LCPs in coincidence with IMFs were measured using 16 single-crystal CsI(Tl) detectors of 3 cm length set around the target at angles between  $\theta_{\text{Lab}} = 27^\circ$  and  $\theta_{\text{Lab}} = 155^\circ$ . Sixteen detectors of the Belgian-French neutron detector array DEMON (Detecteur Modulaire de Neutrons) [40] outside the

target chamber were used to measure neutrons, covering polar angles of  $15^\circ \leq \theta_{\text{IMF-n}} \leq 160^\circ$  between the telescope and the neutron detectors, where  $\theta_{\text{IMF-n}}$  was the opening angle between the IMF telescope and each neutron detector. Since the IMFs were taken inclusively, the angle of the IMF telescope was set carefully to optimize the IMF yields. The consideration was that the angle should be small enough to ensure that sufficient IMF yields were obtained above the detector energy threshold, as well as that the angle should be large enough to minimize contributions from peripheral collisions. For this purpose, simulations of the AMD incorporating with GEMINI [39] were performed. The comparison between the experiment and AMD + GEMINI simulations suggested that the events selected by the IMF triggers at the polar angles within  $15\text{--}25^\circ$  are corresponding to semiviolent collisions (see details in Refs. [30,35]). In order to characterize the fragmenting source to isolate the reaction mechanisms involved in the reaction products, a moving source fit [36] was employed. In the moving source fit for IMFs, the sources were classified as projectile-like (PLF), intermediate-velocity (IV), and target-like (TLF) sources according to the source velocity. For neutrons and LCPs, since the measured angles were greater than  $\theta_{\text{lab}} > 20^\circ$  where the PLF source component had negligible contributions to the spectra, two sources, IV source and TLF source, were used in the moving-source fit. Minuit in the Cern library was used to optimize the four parameters for each source, isotope yield, slope parameter, Coulomb energy, and source velocity. The errors of the isotope yields from the moving source fits were evaluated by performing different optimizations with different initial values within a wide range, including source velocity and energy slope etc, rather than the errors given by the Minuit from the fits, since there were many local minima for the multiple parameter fits. The source characterization enables us to isolate the emitting source and eliminate the interference from the source property (isospin, temperature, and density, among others) deviations [41,42], and therefore only the neutron, LCP and IMF yields from the IV source were considered.

For further investigating the Albergo thermometer and its sequential decay correction, a kinematical focusing technique was employed to evaluate the neutron and LCP yields associated with each isotopically identified IMF to reconstruct the yields of hot primary isotopes with the charge numbers of 3–14 from the IV source of the  $^{64}\text{Zn} + ^{112}\text{Sn}$  system. Following the kinematical focusing technique, the particles emitted from a precursor IMF were designated “correlated” particles, whereas those not emitted from the precursor IMF were designated as “uncorrelated” particles. When correlated particles were emitted from a moving parent of an IMF, whose velocity  $v_{\text{IMF}}$  was approximated by the velocity of the detected trigger IMF, the particles isotropically emitted in the frame of the IMF tended to be kinematically focused into a cone centered along the  $v_{\text{IMF}}$  vector of the detected IMF, unlike the case for uncorrelated particles emitted in the same event. The contribution of the correlated particles was determined by the use of a moving source parametrization and the shape of the uncorrelated spectrum was obtained from the particle velocity spectrum observed in coincidence with Li isotopes which were accompanied by the least number of correlated

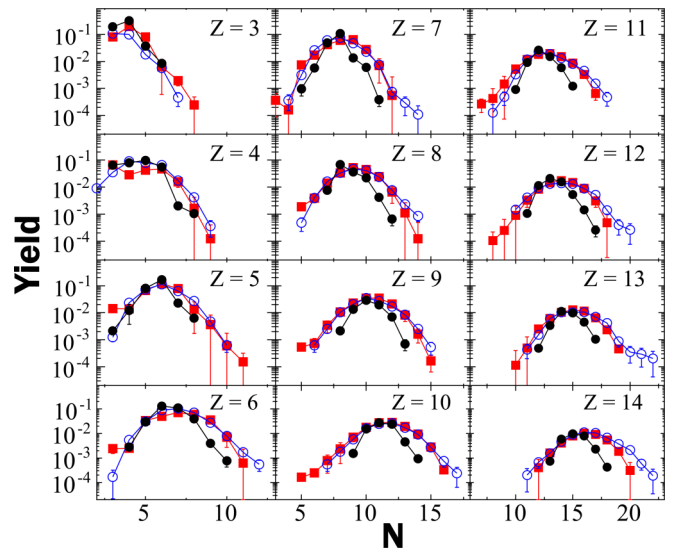


FIG. 1. Yield distributions of the experimentally measured secondary cold fragments (dots) and the reconstructed primary hot IMFs (squares) determined from the collisions of  $^{64}\text{Zn} + ^{112}\text{Sn}$  at 40 MeV/nucleon. The AMD results are plotted by circles for comparison. The figure is taken from Ref. [43] with permission.

particles. Since a part of the light particle emissions in coincidence with the Li isotopes was from the decays of heavier isotopes into light particles and the Li isotopes, and led to an overestimation of the uncorrelated light particle emissions, the correlated particle yields extracted for a given isotope were required to be corrected by the addition of an amount corresponding to the correlated emission of that particle from the Li isotopes evaluated from the AMD-GEMINI simulations [23,39]. The correlated yields were extracted for  $n$ ,  $p$ ,  $d$ ,  $t$ , and  $\alpha$  particles. For the mother nucleus reconstruction, neutron and LCP yields,  $M_i$  ( $i$  is  $n$ ,  $p$ ,  $d$ ,  $t$ , and  $\alpha$ ), were generated for a given cold daughter nucleus on an event-by-event basis, assuming Gaussian distributions with widths evaluated by the GEMINI simulation, and their centroid was adjusted to give the same average yield as that of the experiment. Then the mass and charge of the primary isotope,  $A_{\text{hot}}$ ,  $Z_{\text{hot}}$ , were calculated as  $A_{\text{hot}} = \sum_i M_i A_i + A_{\text{cold}}$  and  $Z_{\text{hot}} = \sum_i M_i Z_i + Z_{\text{cold}}$ , where  $A_i$  and  $Z_i$  are the mass and charge of correlated the particle  $i$ , and  $A_{\text{cold}}$  and  $Z_{\text{cold}}$  are those of the detected cold IMFs. The final results of the measured (dots) and reconstructed primary hot (squares) isotope distributions are compared in Fig. 1. The errors of the reconstructed yields consisted of the errors on the associated neutron and LCP yields from the moving source fit and the errors added for the correction for the emission from the Li isotopes [12]. For some very neutron- or proton-rich isotopes, a larger contribution of the additional error in the reconstructed isotope yield was made from the choice of the input excitation energy for the shape of the neutron and LCP yield distribution calculation with GEMINI [39]. One can see clearly wider isotope distributions for the primary hot IMFs except for  $Z = 3$ , whereas those of the measured IMFs appear much narrower. This demonstrates the significant modification of the yield distributions between the primary hot and the observed cold IMFs caused by

the sequential decay processes. For comparison, the isotope yield distributions from the AMD calculations (see details in Ref. [43]) are also plotted in Fig. 1. It can be observed that the reconstructed primary hot isotope distributions are in close agreement with those from the AMD calculations, suggesting a good performance for constraining the primary hot fragment distributions using kinematical focusing technique for this work.

### III. RESULTS AND DISCUSSION

#### A. Albergo thermometer

Under the assumption that equilibrium may be established between free nucleons and composite fragments contained within a certain freeze-out volume  $V$  and a temperature  $T$ , the density of an isotope with  $A$  nucleons and  $Z$  protons ( $A, Z$ ) may be expressed as

$$\rho(A, Z) = \frac{N(A, Z)}{V} = \frac{A^{3/2} \omega(A, Z)}{\lambda_T^3} \exp\left[\frac{\mu(A, Z) + B(A, Z)}{T}\right], \quad (1)$$

where  $N(A, Z)$  is the number of isotope ( $A, Z$ ) within the volume  $V$ ;  $\lambda_T = h/(2\pi m_0 T)^{1/2}$  is the thermal nucleon wavelength, where  $m_0$  is the nucleon mass;  $B(A, Z)$  is the binding energy;  $\omega(A, Z)$  is the internal partition function of the isotope ( $A, Z$ ) and related to the ground- and excited-state spins as

$$\omega(A, Z) = \sum_j [2s_j(A, Z) + 1] \exp[-E_j(A, Z)/T], \quad (2)$$

where  $s_j(A, Z)$  are ground- and excited-state spins and  $E_j(A, Z)$  are the excitation energies of these states.  $\mu(A, Z)$  in Eq. (1) is the chemical potential of the isotope ( $A, Z$ ). In chemical equilibrium,  $\mu(A, Z)$  is expressed as

$$\mu(A, Z) = Z\mu_p + (A - Z)\mu_n, \quad (3)$$

where  $\mu_p$  and  $\mu_n$  are the chemical potentials of free protons and free neutrons, respectively. Calculating the densities of free protons and neutrons,  $\rho_p$  and  $\rho_n$ , in the same volume using Eqs. (1) and (3), performing transforms to obtain  $\mu_p$  and  $\mu_n$ , and then inserting  $\mu_p$  and  $\mu_n$  back into Eq. (1), one obtains

$$\rho(A, Z) = \frac{N(A, Z)}{V} = \frac{A^{3/2} \omega(A, Z) \lambda_T^{3(A-1)}}{(2s_p + 1)^Z (2s_n + 1)^{A-Z}} \rho_p^Z \rho_n^{A-Z} \exp\left[\frac{B(A, Z)}{T}\right], \quad (4)$$

where  $s_p$  and  $s_n$  are the spins of the free proton and neutron, respectively. The ratio between the measured yields of two different nuclei is then

$$\frac{Y(A, Z)}{Y(A', Z')} = \frac{\rho(A, Z)}{\rho(A', Z')} = \left(\frac{A}{A'}\right)^{3/2} \left(\frac{\lambda_T^3}{2}\right)^{A-A'} \frac{\omega(A, Z)}{\omega(A', Z')} \rho_p^{(Z-Z')} \rho_n^{(A-Z)-(A'-Z')} \exp\left[\frac{B(A, Z) - B(A', Z')}{T}\right]. \quad (5)$$

The free neutron density can be calculated from the yield ratio of two isotopes with only one neutron difference, such as ( $A, Z$ ) and ( $A + 1, Z$ ),

$$\rho_n = C \cdot \left(\frac{A}{A+1} T\right)^{3/2} \frac{\omega(A, Z)}{\omega(A+1, Z)} \exp\left[\frac{B(A, Z) - B(A+1, Z)}{T}\right] \frac{Y(A+1, Z)}{Y(A, Z)}, \quad (6)$$

where  $C$  is the constant related to the unit conversion. Analogously, the free proton density is calculated from the yield ratio of two isotones with only one proton difference, such as ( $A, Z$ ) and ( $A + 1, Z + 1$ ),

$$\rho_p = C \left(\frac{A}{A+1} T\right)^{3/2} \frac{\omega(A, Z)}{\omega(A+1, Z+1)} \exp\left[\frac{B(A, Z) - B(A+1, Z+1)}{T}\right] \frac{Y(A+1, Z+1)}{Y(A, Z)}. \quad (7)$$

The ratio of free proton and neutron densities is calculated from the yield ratio of two isobars with one proton and one neutron difference, such as ( $A, Z$ ) and ( $A, Z + 1$ ),

$$\frac{\rho_p}{\rho_n} = CT^{3/2} \frac{\omega(A, Z)}{\omega(A, Z+1)} \exp\left[\frac{B(A, Z) - B(A, Z+1)}{T}\right] \frac{Y(A, Z+1)}{Y(A, Z)}. \quad (8)$$

For a nuclear system with a given temperature  $T$ , the same free neutron and proton densities and free proton and neutron density ratio must be evaluated from Eqs. (6)–(8). Choosing two isotope, isotone, or isobar ratios with one proton and/or neutron difference, one can deduce the relation between  $T$  and the fragment yield ratios as

$$T = \frac{B}{\ln(aR)}, \quad (9)$$

and the relative error of  $T$ ,  $\delta T/T$ , is deduced as

$$\frac{\delta T}{T} = \frac{1}{\ln(aR)} \frac{\delta R}{R}, \quad (10)$$

where  $R = (Y_1/Y_2)/(Y_3/Y_4)$  is the double yield ratio for (1,2), and (3,4) ratio pairs and  $\delta R$  is the error of  $R$ .  $B$  is the binding energy difference given by  $B = (B_1 - B_2) - (B_3 - B_4)$ , and  $a$

is the statistical weight factor

$$a = \frac{\omega_3/\omega_4}{\omega_1/\omega_2} \left[ \frac{A_3/A_4}{A_1/A_2} \right]^{1.5}. \quad (11)$$

In this work,  $\omega$  is determined with Eq. (2) using all available experimentally measured nuclear levels for a given nucleus. The experimental level scheme for the given nucleus is cited from National Nuclear Data Center (NNDC) [44].

Along with the above formalism of the Albergo thermometer, we deduce the real source temperature and the apparent temperature using yields of the experimentally reconstructed primary hot and measured cold fragments from the  $^{64}\text{Zn} + ^{112}\text{Sn}$  system. Note that  $T$  is used twice in Eqs. (2) and (9), and therefore their values should be deduced consistently. In order to achieve that, an iterative technique is employed. That is, in the first round,  $T = T_1$  MeV is initialized to be 1 MeV in Eq. (2) to calculate the statistical weight factor  $a$ . The resulting  $a$  value is plugged into Eq. (9) to calculate the temperature value  $T'_1$ . In the second round, setting  $T = T_2 = (T_1 + T'_1)/2$  in Eq. (2) to recalculate  $a$  and plugging the new  $a$  into Eq. (9),  $T'_2$  can be then obtained. The iteration continues until  $|T_n - T'_n|/T_n < 1\%$ , where the subscript  $n$  represents the iteration round order. In contrast, if experimentally measured cold fragment yields are used to deduce the apparent temperature, only the ground-state spins of nuclei are taken into account without the iteration procedure practically, following Refs. [11,30,34,35,45]. For a clarity, the real source temperature and the apparent temperature are, respectively, denoted as  $T$  and  $T_{\text{app}}$  hereinafter.

In previous works [11,30,34,35,45], double isotope yield ratio pairs were used to construct the Albergo thermometer. In the present study, all available pairs of double isotope, isotone, and isobar yield ratios with one proton and/or neutron difference within the available primary hot and secondary cold fragment yields of the  $^{64}\text{Zn} + ^{112}\text{Sn}$  system (see Fig. 1) are used to construct the thermometers following the Albergo thermometer formalism. It should be mentioned that the LCP-related thermometers are absent, since the minimum charge number of the reconstructed hot fragments is 3. In Fig. 2(a), the obtained  $T$  values using the constructed thermometers are plotted as a function of the  $T_{\text{app}}$  values. Here the results with the relative errors of  $T$  and  $T_{\text{app}}$  given by Eq. (10) both smaller than 20% are presented. One may see from the figure that the deduced values of  $T$  and  $T_{\text{app}}$  both distribute in a wide region. This wide distribution may originate from two factors. One is the  $B$  value in Eq. (9). When Tsang *et al.* studied the Albergo thermometers using many isotope combinations from the reactions of  $p+\text{Xe}$  ranging from 80 to 350 GeV/c, they realized that the Albergo temperature values with  $B > 10$  MeV show a rather narrow distribution around the average values, whereas those with  $B < 10$  MeV show a much wider distribution [11]. Here we select only the results from thermometers with  $B > 10$  MeV. These results are shown in Fig. 2(b). Indeed, most of the points with  $T < 4$  MeV or  $T_{\text{app}} < 2$  MeV are eliminated, and both  $T$  and  $T_{\text{app}}$  are distributed in a narrower region. However, the  $T$  values still spread significantly from  $\approx 3.5$  to  $\approx 7.5$  MeV. This may originate from the second factor, the statistical weight factor  $a$  in Eq. (9). When the  $a$  value is calculated for

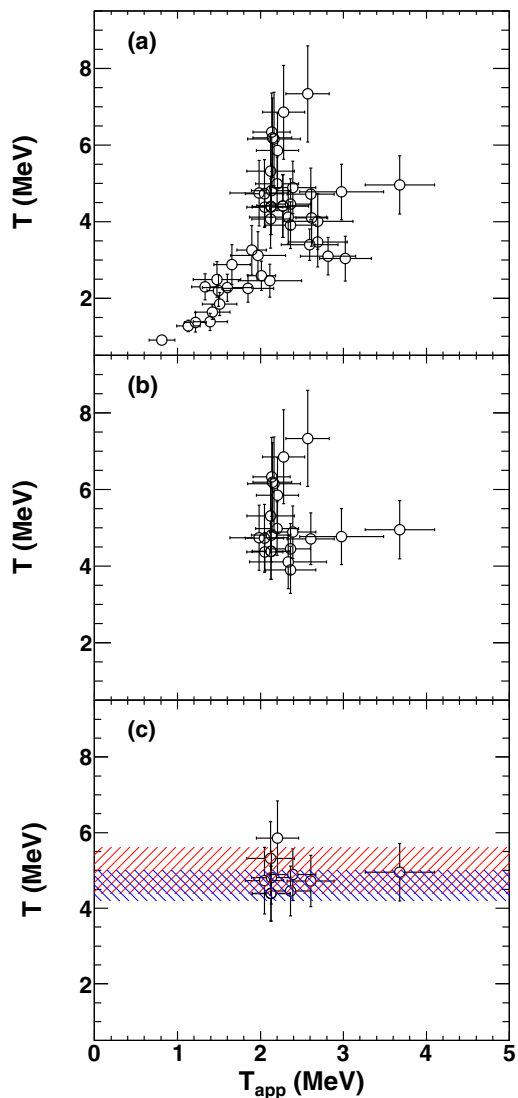


FIG. 2.  $T$ - $T_{\text{app}}$  correlation determined from both primary hot and secondary cold fragment yields from the  $^{64}\text{Zn} + ^{112}\text{Sn}$  system using different Albergo thermometers. (a) The results are deduced from the thermometers constructed using all available pairs of double isotope, isotone, and isobar yield ratios with one proton and/or neutron difference within the present fragment determination region (see Fig. 1) and with a selection of the relative errors of  $T$  and  $T_{\text{app}}$  both smaller than 20%. (b) Same as panel (a), but with a limitation of  $B > 10$  MeV to the thermometers. (c) Same as panel (a), but with both limitations of  $B > 10$  MeV and involved nuclei with the measured maximum excitation levels greater than 1 MeV/nucleon to the thermometers. For comparison, the real temperature values deduced in our two previous works [21,48] are also plotted by shaded areas (see the text).

deducing the  $T$  values, the experimental nuclear level schemes are taken into account. However, the level information is sufficient only for relatively light and stable nuclei. For some heavy nuclei or those slightly far away from the  $\beta$ -stability line, the high excitation levels have not been well determined experimentally, i.e., the excitation level information for  $^{25}\text{Na}$  in NNDC-NuDat 2.8 library [44], for example, is only available up to  $\approx 8$  MeV ( $\lesssim 0.3$  MeV/nucleon). On the other side,

TABLE I. List of the nine thermometers used in Fig. 2(c) and their associated parameters (columns 1–4), the  $T$  and  $T_{\text{app}}$  values deduced from the reconstructed hot and measured cold fragment yields of the  $^{64}\text{Zn} + ^{112}\text{Sn}$  system (columns 5 and 6), and the deduced  $\ln \kappa/B$  values (column 7) using Eq. (12).  $a_{\text{hot}}$  represents the statistical weight factor calculated from all available experimentally measured nuclear levels for a given nucleus, and  $a_{\text{cold}}$  represents the statistical weight factor calculated from the ground-state spins for a given nucleus (see the text).

Isotope Ratio	$B$ (MeV)	$a_{\text{hot}}$	$a_{\text{cold}}$	$T$ (MeV)	$T_{\text{app}}$ (MeV)	$\ln \kappa/B$ (MeV) $^{-1}$
$^{10}\text{Be}^{11}\text{Be} / ^{10}\text{B}^{11}\text{B}$	10.95	3.26	3.50	$4.4 \pm 0.7$	$2.1 \pm 0.2$	0.264
$^{12}\text{C}^{13}\text{N} / ^{11}\text{Be}^{12}\text{B}$	12.17	1.10	1.32	$5.3 \pm 1.0$	$2.1 \pm 0.3$	0.265
$^{10}\text{Be}^{11}\text{Be} / ^{14}\text{N}^{15}\text{N}$	10.33	2.81	3.12	$4.7 \pm 0.9$	$2.1 \pm 0.2$	0.282
$^7\text{Li}^7\text{Be} / ^{11}\text{Be}^{11}\text{B}$	12.37	1.15	0.50	$4.5 \pm 0.7$	$2.4 \pm 0.2$	0.217
$^{11}\text{B}^{11}\text{C} / ^{11}\text{Be}^{11}\text{B}$	13.49	1.05	0.50	$4.7 \pm 0.7$	$2.6 \pm 0.3$	0.178
$^{13}\text{C}^{13}\text{N} / ^{11}\text{Be}^{11}\text{B}$	13.73	0.98	0.50	$4.8 \pm 0.7$	$2.1 \pm 0.2$	0.263
$^{15}\text{N}^{19}\text{O} / ^{11}\text{Be}^{11}\text{B}$	14.27	0.96	0.50	$4.9 \pm 0.7$	$2.4 \pm 0.3$	0.212
$^{17}\text{O}^{17}\text{F} / ^{11}\text{Be}^{11}\text{B}$	14.26	0.68	0.50	$5.9 \pm 1.0$	$2.2 \pm 0.3$	0.247
$^{14}\text{C}^{14}\text{N} / ^{12}\text{B}^{12}\text{C}$	13.22	11.93	9.00	$5.0 \pm 0.8$	$3.7 \pm 0.4$	0.066
Avg.				$4.9 \pm 0.5$	$2.4 \pm 0.5$	

following the Fermi gas assumption, a nuclear temperature of 5 MeV, for example, corresponds to an excitation energy of  $\approx 2$  MeV/nucleon even with a large level density parameter of  $13 \text{ MeV}^{-1}$  [46]. The value of  $\approx 2$  MeV/nucleon is around seven times larger than the excitation energy of the measured maximum level for  $^{25}\text{Na}$ . This significant lack of the high excitation level information may result in the inaccuracy of the  $T$  determination, and therefore nuclei with sufficiently well-known high excitation level schemes are demanded to construct the thermometers to ensure their accuracy. Here, the results from the thermometers with the four nuclei in the two sets of ratio pairs all with the measured maximum excitation levels greater than 1 MeV/nucleon are selected out from Fig. 2(b) and shown in Fig. 2(c). In the figure, only nine data points [around half the number of those in Fig. 2(b)] remain. The ratio pair combinations of the nine thermometers, their associated parameters, and the resulting  $T$  and  $T_{\text{app}}$  values are summarized in the first to the sixth columns of Table I. The  $T$  values from these nine thermometers distribute in a much narrower region than those of Fig. 2(b), evidenced by a  $\chi^2$  analysis [47], that the reduced  $\chi^2$  value,  $\chi^2/N_{\text{point}}$ , significantly decreases from 1.06 for Fig. 2(b) to 0.26 for Fig. 2(c), where  $N_{\text{point}}$  represents the number of data points in each figure. This fact demonstrates a crucial role of high excitation level information in the  $T$  determination.

For comparison, the real temperature values deduced from our two previous works [21,48] are also plotted in Fig. 2(c) by the shaded areas. The temperature of  $5.2 \pm 0.6$  MeV, deduced from the same reconstructed hot IMF yields using a self-consistent method [21], is indicated by the red shaded area. The blue shaded area of  $4.6 \pm 0.4$  MeV is deduced using a chemical potential analysis with a quantum statistical model correction, based on the same set of the data used in this article [48]. Rather good agreement is obtained for the results from the three individual analyses as shown in the figure. The present analysis provides a real temperature of  $4.9 \pm 0.5$  MeV by averaging the real temperature values from the nine thermometers, where the error is evaluated as the standard deviation. In heavy ion collisions at intermediate energies, shortly after the projectile and target make contact, the hottest region of the system reaches high temperatures

in excess of 5 MeV, and as time evolves the system cools down to zero by particle emission and by spatial expansion. It is worth mentioning again that the obtained real temperature of  $4.9 \pm 0.5$  MeV from IMFs probed using the Albergo thermometers here corresponds to late stages when the IMFs become thermally decoupled from the remaining system.

#### IV. b. $N/Z$ ASYMMETRY DEPENDENCE OF TEMPERATURE

In order to study of the  $N/Z$  asymmetry dependence of nuclear temperature, the above nine Albergo thermometers are used as absolute thermometer to deduce the real temperature values using the measured IMF yield data from the other 12 reaction systems,  $^{70}\text{Zn}$ ,  $^{64}\text{Ni}$  on  $^{112,124}\text{Sn}$ ,  $^{58,64}\text{Ni}$ ,  $^{197}\text{Au}$ , and  $^{232}\text{Th}$ . To achieve the sequential decay correction from the apparent temperatures to the real ones for these 12 systems, for which no reconstructed primary hot IMF yields are available, the empirical correction factor (denoted as “ $\ln \kappa/B$ ”) approach of Tsang *et al.* [11] is adopted with the following considerations: (1) to avoid extra assumptions and uncertainties introduced by models and (2) to avoid the dependence of the empirical correction factor on specific reaction systems, incident energies, and fragment pairs used. The above deduced real temperature from the yields of the experimentally reconstructed primary hot fragments from the  $^{64}\text{Zn} + ^{112}\text{Sn}$  system [12] provides such an opportunity to deduce the certain  $\ln \kappa/B$  values for the reaction systems involved in this work. According to Ref. [45], Xi *et al.* found that the  $\ln \kappa/B$  value for a given thermometer at temperatures around 4.5 MeV (similar to that of the present work,  $4.9 \pm 0.5$  MeV) is independent of the projectile-target combination of reactions, providing us a justification for the application of the  $\ln \kappa/B$  values obtained from one system of  $^{64}\text{Zn} + ^{112}\text{Sn}$  to the other 12 systems with different  $N/Z$  asymmetries. The average temperature value of  $4.9 \pm 0.5$  MeV for the system of  $^{64}\text{Zn} + ^{112}\text{Sn}$  is therefore taken to evaluate the  $\ln \kappa/B$  values for the nine thermometers, based on the relation between the real temperature and the

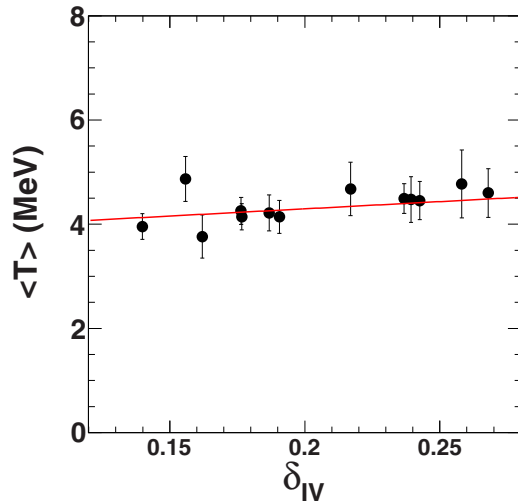


FIG. 3. Average temperature  $\langle T \rangle$  as a function of source  $N/Z$  asymmetry  $\delta_{IV}$ . Solid line is the linear fit of the data points.

apparent temperature [11],

$$\frac{1}{T} = \frac{1}{T_{\text{app}}} - \frac{\ln \kappa}{B}. \quad (12)$$

The resultant  $\ln \kappa/B$  values are listed in the seventh column of Table 1.

The sequential decay corrections for the apparent temperatures deduced from the 12 systems,  $^{70}\text{Zn}$ ,  $^{64}\text{Ni}$  on  $^{112,124}\text{Sn}$ ,  $^{58,64}\text{Ni}$ ,  $^{197}\text{Au}$ , and  $^{232}\text{Th}$ , are performed using the obtained  $\ln \kappa/B$  values from the  $^{64}\text{Zn} + ^{112}\text{Sn}$  system. For each given system, the average real source temperature value,  $\langle T \rangle$ , is calculated as an average value over the real temperature values corrected for the nine thermometers. In Fig. 3, the resulting  $\langle T \rangle$  values for the 13 systems are shown as a function of the IV source  $N/Z$  asymmetry,  $\delta_{IV} = (N_{IV} - Z_{IV})/A_{IV}$ , where  $N_{IV}$ ,  $Z_{IV}$ , and  $A_{IV}$  are the neutron, proton, and mass of the fragmenting source calculated from summing over the experimentally measured IV component yields of neutrons, LCPs, and IMFs with  $Z$  up to 18. The errors shown in the figure are the standard deviations only. A linear fit is performed for the  $\langle T \rangle$  versus  $\delta_{IV}$  plot, and a slope of 3 MeV is obtained. An change in source  $N/Z$  asymmetry of 0.1 unit corresponds to a absolute change in temperature on the order of 0.3 MeV, indicating a rather negligible  $N/Z$  asymmetry dependence of the real temperature at the present source  $N/Z$  range. It should be mentioned that the source mass has a negligible contribution to the present observation, since no significant size dependence was experimentally observed for the reactions with system sizes and incident energies similar to those of this work [49]. This conclusion is in a close agreement with those of our previous works [30,35], in which the Albero thermometer was used as a relative thermometer, and an “indirect” method of Sfienti *et al.* [37] was adopted to consider the sequential decay effect. This consistency suggests that the resulting negligible  $N/Z$  asymmetry dependence of nuclear temperature is insensitive to the selection of sequential decay correction. The negligible  $N/Z$  asymmetry dependence of nuclear temperature from IMFs is in close agreement with the

theoretical predictions by Kolomietz *et al.* [50,51] and Hoel *et al.* [31]. Kolomietz *et al.* studied the dependence of the plateau temperature in caloric curves on pressure within the thermal Thomas-Fermi approximation and found that a weak  $N/Z$  asymmetry dependence of temperature close to the phase transition appears under an equilibrium at a low pressure of  $p = 10^{-2} \text{ MeV/fm}^3$  for systems with asymmetries of 0–0.3 (covering the present source asymmetry region). Later, Hoel *et al.* studied the asymmetry dependence of caloric curve for mononucleus with asymmetries of 0.1–0.4 using a model with specific consideration for independent variation of the neutron and proton surface diffusenesses. They found that the asymmetry dependence of caloric curve could be removed while using the unique boundary condition with equilibrated surface and no external pressure. In spite of being in completely different frameworks, both theoretical predictions reflect that the apparent asymmetry dependence of nuclear temperature is related to the pressure of system. In actual heavy-ion collisions, the low-pressure condition can be more or less satisfied in the IMF formation scenario at late stages and under low densities. It is therefore reasonable to infer that the negligible  $N/Z$  asymmetry dependence of nuclear temperature from IMFs originates from a process that occurs at a low pressure via a “soft” expansion.

We have also made detailed comparisons between the available experimental results and ours deduced from LCP and IMF yields in Refs. [30,35]. Those comparisons show that a weak  $N/Z$  asymmetry dependence of nuclear temperature is commonly observed in different reactions and with different thermometers at a wide  $N/Z$  range [7,37,52], except for the result reported by McIntosh *et al.* [29]. We noticed that, unlike others, Wuenschel *et al.* [7] and McIntosh *et al.* [29] both used the same proton quadrupole momentum fluctuation thermometer as a probe. With close examination of the experimental details of Wuenschel *et al.* and McIntosh *et al.* and combined with the statistical multifragmentation model simulations [38], we concluded that the significant  $N/Z$  dependence of the source temperature observed by McIntosh *et al.* originates from different Coulomb contributions in the reconstructed quasiprojectiles with different charges under the quasiprojectile mass constraint. After properly taking into account the Coulomb effect, the  $N/Z$  dependence of the source temperature again becomes insignificant. Therefore, it can be concluded that nuclear temperature has a negligible dependence on the source  $N/Z$  asymmetry in this asymmetry range, and the negligible  $N/Z$  asymmetry dependence is also independent of the selections of the thermometers. The consistent description for the  $N/Z$  asymmetry dependence of nuclear temperature provides evidence supporting the basic assumption of  $N/Z$  asymmetry independence of the source temperature in the symmetry energy extraction using isoscaling in the heavy-ion collisions at Fermi energies [41,53]. Although good consistency of the dependence of nuclear temperature on the source  $N/Z$  asymmetry has been experimentally addressed using different thermometers in a wide incident energy region, the origin of the common negligible  $N/Z$  asymmetry dependence of nuclear temperature from LCPs and those deduced using fluctuation thermometers is still not addressed for the present work. Difficulties comes

from the complicated reaction dynamics and different application limitations of various thermometers. For instance, in contrast to IMFs, the emissions of LCPs start to occur shortly after the projectile and target make contact and lasts in the overall dynamical process. The negligible  $N/Z$  asymmetry dependence of nuclear temperature is not able to be elucidated using simply using the “low-pressure” assumption [31,50,51]. In addition, the Albergo thermometers probe the temperatures at the chemical freeze-out, whereas the fluctuation thermometers are for those at thermal freeze-out, while it has been found that chemical freeze-out occurs prior to thermal freeze-out during source fragmentations [10]. Therefore, to better understand the mechanism resulting in the consistent  $N/Z$  dependence of nuclear temperature, specific considerations for the reaction dynamics and the thermometer limitations are required in future experimental and theoretical works.

## V. SUMMARY

In this article, the Albergo thermometer is investigated using the yields of the experimentally measured and reconstructed primary hot IMFs from  $^{64}\text{Zn} + ^{112}\text{Sn}$  collisions at 40 MeV/nucleon for the first time. A real temperature value of  $4.9 \pm 0.5$  MeV characterizing the IMF formation at late stages is deduced. This temperature value is in good agreement with those obtained in our two previous works, i.e.,  $5.2 \pm 0.6$  MeV deduced from the same reconstructed hot IMF yields using a self-consistent method [21], and  $4.6 \pm 0.4$  MeV deduced using a chemical potential analysis with a quantum statistical model correction [48]. Using the center temperature value, 4.9 MeV of the present work, an experimental sequential decay correction from the apparent temperatures to the real ones for 12 other reaction systems with different  $N/Z$  asymmetries,  $^{70}\text{Zn}$ ,  $^{64}\text{Ni}$  on  $^{112,124}\text{Sn}$ ,  $^{58,64}\text{Ni}$ ,  $^{197}\text{Au}$ , and  $^{232}\text{Th}$  at 40 MeV/nucleon in the same experiment, is performed with an empirical correction factor approach of Tsang *et al.* [11], and the dependence of nuclear temperature on the source  $N/Z$

asymmetry is further investigated. It is found that the deduced real source temperatures show a rather weak dependence on the source  $N/Z$  asymmetry at the present source  $N/Z$  range. Combining the theoretical predictions by Kolomietz *et al.* [50,51] and Hoel *et al.* [31], the negligible  $N/Z$  asymmetry dependence of nuclear temperature from IMFs is inferred to originate from a process that occurs at a low pressure via a “soft” expansion. From comparisons with our previous results and those from other independent experiments, a consistent description for the  $N/Z$  asymmetry dependence of nuclear temperature is obtained. That is, nuclear temperature has a negligible dependence on the source  $N/Z$  asymmetry, and this negligible  $N/Z$  asymmetry dependence is independent of the selections of the thermometers and the sequential decay correction approaches. This supports the assumption of  $N/Z$  asymmetry independence of the source temperature in the symmetry energy extraction using isoscaling in heavy-ion collisions at Fermi energies [41,53]. In spite of good consistency of the dependence of nuclear temperature on the source  $N/Z$  asymmetry, the origin of the negligible  $N/Z$  asymmetry dependence of nuclear temperature from LCPs and those deduced using fluctuation thermometers is still an open question for this work. To fully clarify this issue, the reaction dynamics and the thermometer limitations are required in future experimental and theoretical investigation on the  $N/Z$  asymmetry of nuclear temperature.

## ACKNOWLEDGMENTS

The authors thank the operational staff in the Cyclotron Institute, Texas A&M University, for their support during the experiment. This work is supported by the National Natural Science Foundation of China (Grants No. 11705242, No. U1632138, No. 11805138, and No. 11905120) and the Fundamental Research Funds for the Central Universities (Grants No. YJ201954, No. YJ201820, and No. GK201903022) in China. This work is also supported by the US Department of Energy under Grant No. DE-FG02-93ER40773.

- 
- [1] H. A. Bethe, *Rev. Mod. Phys.* **9**, 69 (1937).
  - [2] V. F. Weisskopf, *Phys. Rev.* **52**, 295 (1937).
  - [3] A. Kelić, J. B. Natowitz, and K.-H. Schmidt, *Eur. Phys. J. A* **30**, 203 (2006).
  - [4] E. Suraud, C. Grégoire, and B. Tamain, *Prog. Part. Nucl. Phys.* **23**, 357 (1989).
  - [5] G. D. Westfall, B. V. Jacak, N. Anantaraman, M. W. Curtin, G. M. Crawley, C. K. Gelbke, B. Hasselquist, W. G. Lynch, D. K. Scott, B. M. Tsang *et al.*, *Phys. Lett. B* **116**, 118 (1982).
  - [6] B. V. Jacak, G. D. Westfall, C. K. Gelbke, L. H. Harwood, W. G. Lynch, D. K. Scott, H. Stocker, M. B. Tsang, and T. J. M. Symons, *Phys. Rev. Lett.* **51**, 1846 (1983).
  - [7] S. Wuenschel, A. Bonasera, L. W. May, G. A. Souliotis, R. Tripathi, S. Galanopoulos, Z. Kohley, K. Hagel, D. V. Shetty, K. Huseman *et al.*, *Nucl. Phys. A* **843**, 1 (2010).
  - [8] S. Albergo, S. Costa, E. Costanzo, and A. Rubbino, *Nuovo Cimento A* **89**, 1 (1985).
  - [9] D. J. Morrissey, W. Benenson, E. Kashy, B. Sherrill, A. D. Panagiotou, R. A. Blue, R. M. Ronningen, J. van der Plicht, and H. Utsunomiya, *Phys. Lett. B* **148**, 423 (1984).
  - [10] W. Trautmann *et al.* (ALADIN Collaboration), *Phys. Rev. C* **76**, 064606 (2007).
  - [11] M. B. Tsang, W. G. Lynch, H. Xi, and W. A. Friedman, *Phys. Rev. Lett.* **78**, 3836 (1997).
  - [12] M. R. D. Rodrigues, W. Lin, X. Liu, M. Huang, S. Zhang, Z. Chen, J. Wang, R. Wada, S. Kowalski, T. Keutgen, K. Hagel, M. Barbui, C. Bottosso, A. Bonasera, J. B. Natowitz, T. Materna, L. Qin, P. K. Sahu, and K. J. Schmidt, *Phys. Rev. C* **88**, 034605 (2013).
  - [13] K. Hagel, M. Gonin, R. Wada, J. B. Natowitz, B. H. Sa, Y. Lou, M. Gui, D. Utley, G. Nebbia, D. Fabris, G. Prete, J. Ruiz, D. Drain, B. Chambon, B. Cheynis, D. Guinet, X. C. Hu, A. Demeyer, C. Pastor, A. Giorni, A. Lleres, P. Stassi, J. B. Viano, and P. Gonthier, *Phys. Rev. Lett.* **68**, 2141 (1992).
  - [14] A. Ono and H. Horiuchi, *Phys. Rev. C* **53**, 2958 (1996).
  - [15] C. Schwarz, S. Fritz, R. Bassini, M. Begemann-Blaich, S. J. Gaff-Ejakov, D. Gourio, C. Groß, G. Immé, I. Iori, U. Kleinevoß *et al.*, *Nucl. Phys. A* **681**, 279 (2001).
  - [16] B. Borderie and M. F. Rivet, *Prog. Part. Nucl. Phys.* **61**, 551 (2008).



- [17] H. Xi, W. G. Lynch, M. B. Tsang, W. A. Friedman, and D. Durand, *Phys. Rev. C* **59**, 1567 (1999).
- [18] T. C. Awes, G. Poggi, C. K. Gelbke, B. B. Back, B. G. Glagola, H. Breuer, and V. E. Viola, *Phys. Rev. C* **89**, 021601(R) (2014).
- [19] X. Liu, W. Lin, R. Wada, M. Huang, Z. Chen, G. Q. Xiao, S. Zhang, X. Jin, R. Han, J. Liu, F. Shi, H. Zheng, J. B. Natowitz, and A. Bonasera, *Phys. Rev. C* **90**, 014605 (2014).
- [20] X. Liu, W. Lin, R. Wada, M. Huang, P. Ren, Z. Chen, J. Wang, G. Q. Xiao, S. Zhang, H. Rui *et al.*, *Nucl. Phys. A* **933**, 290 (2015).
- [21] X. Liu, H. Zheng, W. Lin, M. Huang, Y. Y. Yang, J. S. Wang, R. Wada, A. Bonasera, and J. B. Natowitz, *Phys. Rev. C* **97**, 014613 (2018).
- [22] X. Liu, W. Lin, M. Huang, R. Wada, J. Wang, Z. Chen, Q. Wang, P. Ren, Y. Yang, S. Jin, P. Ma, J. Ma, Z. Bai, and Q. Hu, *Phys. Rev. C* **92**, 014623 (2015).
- [23] A. Ono, *Phys. Rev. C* **59**, 853 (1999).
- [24] W. A. Friedman, *Phys. Rev. Lett.* **60**, 2125 (1988).
- [25] D. Gross, *Prog. Part. Nucl. Phys.* **30**, 155 (1993).
- [26] Bao-An Li, Lie-Wen Chen, and Che Ming Ko, *Phys. Rep.* **464**, 113 (2008).
- [27] G. Giuliani, H. Zheng, and A. Bonasera, *Prog. Part. Nucl. Phys.* **76**, 116 (2014).
- [28] C. Guo, J. Su, and F. Zhang, *Nucl. Sci. and Tech.* **24**, 050513 (2013).
- [29] A. B. McIntosh, A. Bonasera, P. Cammarata, K. Hagel, L. Heilborn, Z. Kohley, J. Mabiala, L. W. May, P. Marini, A. Raphelt *et al.*, *Phys. Lett. B* **719**, 337 (2013).
- [30] Y. Huang, W. Lin, H. Zheng, R. Wada, X. Liu, G. Qu, M. Huang, P. Ren, J. Han, M. R. D. Rodrigues, S. Kowalski, T. Keutgen, K. Hagel, M. Barbui, A. Bonasera, and J. B. Natowitz, *Phys. Rev. C* **101**, 064603 (2020).
- [31] C. Hoel, L. G. Sobotka, and R. J. Charity, *Phys. Rev. C* **75**, 017601 (2007).
- [32] J. Besprosvany and S. Levit, *Phys. Lett. B* **217**, 1 (1989).
- [33] R. Ogul and A. S. Botvina, *Phys. Rev. C* **66**, 051601(R) (2002).
- [34] J. Su and F. S. Zhang, *Phys. Rev. C* **84**, 037601 (2011).
- [35] X. Liu, H. Zheng, R. Wada, W. Lin, M. Huang, P. Ren, G. Qu, J. Han, M. R. D. Rodrigues, S. Kowalski, T. Keutgen, K. Hagel *et al.*, *Phys. Rev. C* **100**, 064601 (2019).
- [36] T. C. Awes, G. Poggi, C. K. Gelbke, B. B. Back, B. G. Glagola, H. Breuer, and V. E. Viola, Jr., *Phys. Rev. C* **24**, 89 (1981).
- [37] C. Sienti, P. Adrich, T. Aumann, C. O. Bacri, T. Barczyk, R. Bassini, S. Bianchin, C. Boiano, A. S. Botvina, A. Boudard *et al.*, *Phys. Rev. Lett.* **102**, 152701 (2009).
- [38] J. Bondorf, A. S. Botvina, A. S. Ijtinov, I. N. Mishutin, and K. Sneppen, *Phys. Rep.* **257**, 133 (1995).
- [39] R. J. Charity, A. McMahan, G. J. Wozniak, R. J. McDonald, L. G. Moretto, D. G. Sarantites, L. G. Sobotka, G. Guarino, A. Pantaleo, L. Fiore, A. Gobbi, and K. D. Hildenbrand, *Nucl. Phys. A* **483**, 371 (1988).
- [40] I. Tilquin, Y. El Masri, M. Parlog, Ph. Collon, M. Hadri, Th. Keutgen, J. Lehmann, P. Leleux, P. Lipnik, A. Ninane *et al.*, *Nucl. Instrum. Methods A* **365**, 446 (1995).
- [41] H. S. Xu, M. B. Tsang, T. X. Liu, X. D. Liu, W. G. Lynch, W. P. Tan, A. Vander Molen, G. Verde, A. Wagner, H. F. Xi, C. K. Gelbke, L. Beaulieu, B. Davin, Y. Larochele, T. Lefort, R. T. de Souza, R. Yanez, V. E. Viola, R. J. Charity, and L. G. Sobotka, *Phys. Rev. Lett.* **85**, 716 (2000).
- [42] M. B. Tsang, T. X. Liu, L. Shi, P. Danielewicz, C. K. Gelbke, X. D. Liu, W. G. Lynch, W. P. Tan, G. Verde, A. Wagner *et al.*, *Phys. Rev. Lett.* **92**, 062701 (2004).
- [43] W. Lin, X. Liu, M. R. D. Rodrigues, S. Kowalski, R. Wada, M. Huang, S. Zhang, Z. Chen, J. Wang, G. Q. Xiao, R. Han, Z. Jin, J. Liu *et al.*, *Phys. Rev. C* **90**, 044603 (2014).
- [44] <https://www.nndc.bnl.gov/nudat2>
- [45] H. Xi *et al.* (Miniball/Multics Collaboration), *Phys. Lett. B* **431**, 8 (1998).
- [46] J. B. Natowitz, R. Wada, K. Hagel, T. Keutgen, M. Murray, A. Makeev, L. Qin, P. Smith, and C. Hamilton, *Phys. Rev. C* **65**, 034618 (2002).
- [47] F. Zhu, W. G. Lynch, D. R. Bowman, R. T. de Souza, C. K. Gelbke, Y. D. Kim, L. Phair, M. B. Tsang, C. Williams, and H. M. Xu, *Phys. Rev. C* **52**, 784 (1995).
- [48] X. Liu, W. Lin, M. Huang, R. Wada, J. Wang, A. Bonasera, H. Zheng, Z. Chen, S. Kowalski, T. Keutgen, K. Hagel, L. Qin, J. B. Natowitz, T. Materna, P. K. Sahu, M. Barbui, C. Bottosso, and M. R. D. Rodrigues, *Phys. Rev. C* **95**, 044601 (2017).
- [49] J. Wang *et al.* (NIMROD Collaboration), *Phys. Rev. C* **72**, 024603 (2005).
- [50] V. M. Kolomietz, A. I. Sanzhur, S. Shlomo, and S. A. Firin, *Phys. Rev. C* **64**, 024315 (2001).
- [51] S. Shlomo and V. M. Kolomietz, *Rep. Prog. Phys.* **68**, 1 (2005).
- [52] G. J. Kunde, S. Gaff, C. K. Gelbke, T. Glasmacher, M. J. Huang, R. Lemmon, W. G. Lynch, L. Manduci, L. Martin, M. B. Tsang *et al.*, *Phys. Lett. B* **416**, 56 (1998).
- [53] M. B. Tsang, C. K. Gelbke, X. D. Liu, W. G. Lynch, W. P. Tan, G. Verde, H. S. Xu, W. A. Friedman, R. Donangelo, S. R. Souza, C. B. Das, S. Das Gupta, and D. Zhabinsky, *Phys. Rev. C* **64**, 054615 (2001).